Investigation of Properties, Nanostructure, and Distribution in Controlled Polyester Polymerization with Layered Silicate

YANG-CHUAN KE,[1] ZHI-BIN YANG,[1] CHUAN-FENG ZHU[2]

[1] Polyolefin National Engineering Research Center, BRICI, Sinopec, People's Republic of China 100013

[2] Institute of Chemistry, Chinese Academy of Sciences, People's Republic of China, 100085

Received 16 March 2001; accepted 4 October 2001

ABSTRACT: This article presents a series of nanocomposites of a polyester [poly(ethylene terephathalate), PET] with different contents of layered silicates of montmorillonite (MMt) by a controlled process, that is, controlling the way to pretreat MMt, the content of MMt, the kind of reagents used, and the way for MMt to be added. Also investigated, in detail, were the properties, nanostructure, and distribution of nanocomposites with an MMt content below 5% by weight. Results by TEM and AFM showed that the nanoparticles are in a normal distribution with a most probable size of 30–70 nm; the exfoliated MMt lamellae interacting with the PET molecular chain produced more regular chain patterns than did pure PET itself when the MMt content was low (lower than 3% by weight); and the agglomerated particles seem not to be found in an MMt content less than 3% by weight, but to increase with the MMt content in the nanocomposites. The investigation of these nanocomposite properties showed that the optimized properties require an optimized MMt content within 2–3% by weight. When MMt is increased from 3 to 5% by weight in the nanocomposites, agglomeration is unavoidable. Thus, the critical content for MMt added to PET is about 3% by weight. X-ray results showed the appearance of several small diffraction peaks in the 2θ angle from 1° to 7° for the annealing nanocomposite samples; these peaks are thought to be from the residue of unexfoliated MMt lamellae or metastable (unstable) MMt lamellae. DSC results proved that the nanocomposites have a higher crystallization rate than that of pure PET due to an exfoliated MMt lamellae nucleation effect. Thus, to obtain a stable nanostructure (or nanocomposite), the MMt content needs to be controlled. The nanostructure plays such a role in the crystallization nucleation of nanocomposites. The interaction of exfoliated lamellae with the molecular chain causes a more regular chain pattern and affects the PET crystallization rate and morphology. © 2002 Wiley Periodicals, Inc. J Appl Polym Sci 85: 2677–2691, 2002

Key words: nanocomposites; polyesters; layered clay; crystallization; nanostructure

INTRODUCTION

Nanoscale materials and technologies are attracting great attention from investigators worldwide due to their potential application to many fields, such as for electronics parts, optical fiber, robots, the coating industry, catalysts, biomaterials , biomedical materials, and the life sciences.[1–3] Current nanotechnologies and nanoscale materials are used in many traditional industries, which has led to smaller-scale integrated circuits and catalysts,[3,4] while the traditional organic polymer properties are enhanced. In fact, modifications of an organic polymer fiber texture via this technology have resulted in keeping energy from dissi-

Correspondence to: Y.-C. Ke, No. 14 East Road of BeiSanHuan, Beujing Research Institute of Chemical Industry, Beijing, People's Republic of China 10013 (ycke@brici.ac.cn).

Contract grant sponsor: BASF Co.

Contract grant sponsor: Ministry of Science and Technology; contract grant number: 1999064800.

Journal of Applied Polymer Science, Vol. 85, 2677–2691 (2002)

Table I Nanocomposite Properties Judged from Some of the Characterization Items Obtained from the Difference Between the Nanocomposites and Their Pure Counterparts

Sample	DHDT (°C)	$T_c - T_g$ (°C)	σ_b and σ_t	Optical Properties
PET/MMt	20–50	90	Not bad	Better
PBT/MMt	20–50	70	Good	Little better
PA/MMt	50–100		Good	Better
PE/MMt			Good	Little better

dHDT, heat-distortion temperature difference between nanocomposite samples and their pure matrix counterparts; $T_c - T_g$, difference between temperature of sample crystallized from the melt state (T_c) and the glassy state temperature (T_g); σ_b and σ_t, bending strength and tensile strength, respectively; optical properities, comparison results for samples subject to visible light (400–800 nm).

pating, and mechanical and thermal properties have been enhanced significantly by only loading a small amount of inorganic nanoparticles.[5–10] In fiber and film applications of organic polymers, many different ways to keep fiber products (e.g., clothes) warm after a quick heat loss and to decrease the permeability value of organic films to gas such as O_2, CO_2, and N_2 have been suggested as well as practiced.

In pioneering practices, the easy and convenient way to modify organic polymers was via the blending of inorganic particles with an organic polymer matrix. For example, to improve the properties of fibers and films of organic polymers as stated above, micron-scale particles of ZrO_2, TiO_2, and SiO_2 were blended into an organic polymer matrix.[5–15] But this blending technology introduced several problems such as phase separation between the inorganic and organic phases, particle agglomerations, and their heterogeneous distribution in blending materials. Nowadays, to avoid such problems, the inorganic phase is not directly introduced into the organic matrix. At present, the inorganic precursor compound is often introduced into an organic matrix, thus reacting with organic molecules, and then the produced inorganic particles are *in situ* distributed in the composites. If the inorganic particle scale produced in these composites is less than 100 nm, the obtained composites are called nanocomposites.

So far, there have been many successful examples of polymer/inorganic nanocomposites reported, from which one of the most active research fields has developed into a new material field called polymers/layered clay nanocomposites or hybrids. These have been reported as nanocomposites of polyamide6/clay (PA6/clay hybrids),[16–20] polystyrene/clay (PS/clay),[21,22] poly(ethylene terephathalate)/clay (PET/clay),[23,24] poly(butylene terephathalate)/clay (PBT/clay),[25] polypropylene/clay (PP/clay), and polyethylene/clay (PE/clay)[10] by an intercalation polymerization process, through which the particles *in situ* distribute in a polymer matrix as soon as their formation in the reaction.

In observing these previous works,[10,23–27,30–35] a series of nanocomposites with improved properties (see Table I), including PET–montmorrillonite (MMt) nanocomposites, have been reported. These materials have partly improved the properties of the polymer matrix with nanoscale particles homogeneously distributed in the matrix, as reported. Also, different technologies[36–45] have been designed to improve the particle distribution, particle bonding interaction with the matrix, and the crystallization morphology. A review of these nanocomposite reports reached the conclusion that the nanostructure (or, as called by Lincoln,[44] a secondary structure in the PA/clay nanocomposite) formed in these nanocomposite samples has a major effect on the polymer matrix properties. This nanostructure is a result of polymer chains reacting or interacting with organic clay particles or a structure of polymer chain bonding with a hierachy of the lamellae of clay in the nanoscale. From some of these reports, it is seen that the heterogeneous nanostructure was often formed in nanocomposites by blending nanoparticles with the polymer matrix, while the homogeneous nanostructure often was formed in nanocomposites by an *in situ* intercalation polymerization process or by a melt-intercalation process.[10,16–22–27,42,44,45]

Due to different views on the nanostructure role in the interaction of polymer chains with inorganic lamellae and the properties enhanced in nanocomposites, in this article, we present just some of our viewpoints for explaining the structure–property relationship, as an overall understanding these polymer/clay nanocomposites has been, so far, difficult. One of the viewpoints on the enhanced properties of a polymer/MMt nanocomposite is that the polymer brushes that interact with the MMt lamellae may control the nanoscale distribution or morphology and, in turn, the properties of the nanocomposites.[16,32,33] These investigations also proved that the orientation of the silicate layers dictates the orientation of the crystal phase or morphology. Our series of investigations on polymer/MMt nanocomposites revealed that a nanostructure formed by inorganic lamellae with polymer chains controlled their property enhancements,[23–27] which is similar to Lincoln's study in that the crystallite morphology depends on the secondary structure and interfacial interactions[44] and also that the ordered silicate lamellae morphology may be disrupted by too high an MMt content. In fact, Jimenez et al.,[47] Qi et al.,[20] and we[27] found that the MMt layers affect not only the formation of the lamellae but also the spherulites, proved by SAXS evidence.

Some of these above previous reports gave an impression of the capability to prepare perfect nanocomposites with modified clay of MMt under versatile conditions and technologies. But the defects in nanocomposites were not clarified or stressed. For example, the small number of agglomeration particles existing in a polymer matrix (e.g., in PET/clay nanocomposites) produced a poor appearance, that is, some black particles or yellow-colored dots in the matrix of PET or PA. While the reasons for the production of particle agglomeration have not been clarified yet, a few attempts to get rid of these agglomerations are presented based on preparation routes.[23–27]

In this article, a new method for controlling the clay treatment to obtain PET/MMt nanocomposites is presented. The main objectives were to determine (1) how to control the agglomerations (or distribution), (2) how the controlling process improves the nanocomposite properties, and (3) what nanostructures affect their properties. For these reasons, the investigations cited many previous viewpoints as stated above to explain the structure–property relationship, and, thus, the structure investigations included the nanostructure formation and its effect on the properties of the final nanocomposites.

EXPERIMENTAL

Sample Preparation

The original clay was supplied by the same resources as in refs. 22 and 24, with approximately an 80% content of MMt ore. Its cation-exchange capacity ranges from 70 to 110 meq/100 g. The raw MMt is smashed into particles of 40 μm through a sieve by a mill process after being dehydrated so that the water content was less than 5% by weight The MMt used in this article was treated to a water content of less than 5% by weight, and then the MMt reacted with the organic reagents selected. The organic reagents were selected from the literature,[27] including quaternary ammonium salts with more than six carbons according to their end group and polarities.

Preparation Process of Polyester-layered Silicate Nanocomposites

Clay Pretreatment

In the first step, phosphorous acid is used as the reagent of hydration, which reacts with amine to obtain ammonia salt. Details of this reaction were presented in previous articles.[23–26,32–36] This ammonia salt then is used in the pretreatment of the clay. For example, 0.1 meq of the ammonia salt of laurilamine with phosphorous acid (28.1 g) is dissolved in 200 mL distilled hot water (preheated to 60°C) and then dipped into 125 g powder clay in 1875 mL of water in a 3000-mL flask at 80°C. The obtained mixture is then stirred vigorously for 2 h. Next, the mixture is put into a steel autoclave overnight at 160°C with autogeneous pressure. Also, the obtained slurry is put into a device in which water is drained out to the expected stage with pump air pressure. This process will produce cakes, which are put into a beaker, to which another 300 mL of ethanol is added, and the mixture is broken by a common ultrasonic wave. The obtained final mixture, which contains about 120 g of clay, provides the pretreatment clay used for the following polymerization. The obtained organoclays treated by some different reagents and the original clay characterized by WAXD are shown in Figure 1.

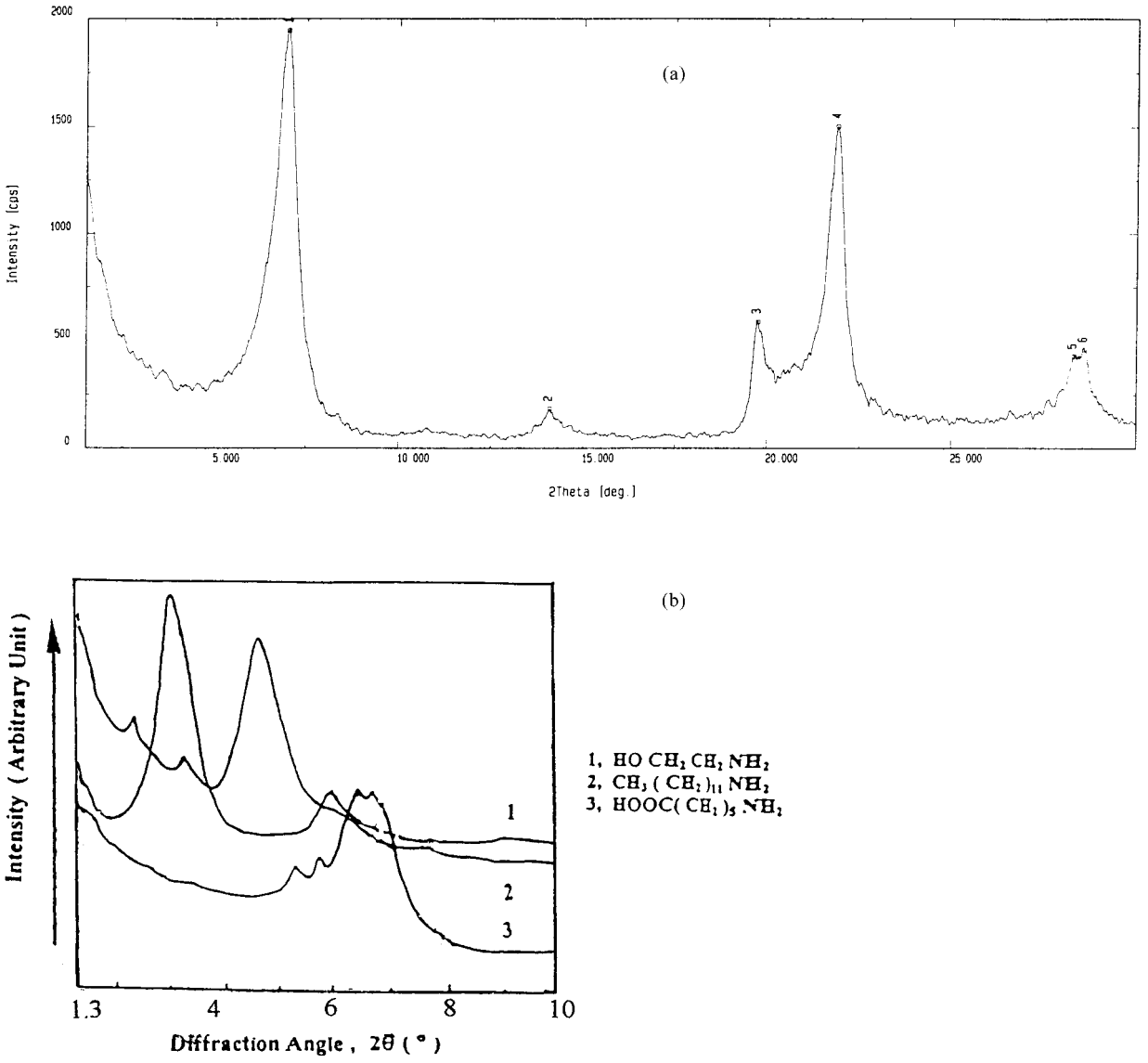

Figure 1 WAXD patterns of (a) original clay and (b) pretreated clay by reagents.

Polymerization

Polymerization was done in a 10-L autoclave. Bihexaneethannolterephathalate (BHET200) oligomers, 4000 g, are melted first; then, 120 g of above pretreatment clay gel is blown into the melt step by step with uniformity within 30 min. Meanwhile, the water, ethaneol, diol, or oligomers are discharged under nitrogen (N_2). During this process, the temperature increases gradually from 230 to 270°C for 30–60 min. The melted mixture (must be clear) and then is kept under a vacuum of 40–80 Pa for about 2 h of polymerization. After that, N_2 is used to squeeze the melt in the shape of strips; then, they are cut into pellets under cold water. The pellets are vacuum-dried at 70°C to obtain the required samples. The characterization results of PET/clay nanocomposites (NPET) are shown in later figures (see, e.g., Fig. 9).

Characterization

Samples obtained in the preparation process are solved in solvents of 50/50 (w/w) of 1,1,2,2-tetracholoroethanephenol and are then measured with an Ulman viscometer with a concentration of 0.1 g/100 mL. These obtained solutions are further diluted into 1/10 of their original concentrations by a $CHCl_3$ solvent and then measured on a

Shimidazu GPC for measurement of their molecular weights. In the measurements, the standard oligomers of PET and the correction test are adapted to analyze the final results. The correction tests are based mainly on the clay content.

WAXD measuring diffraction patterns of the samples was done on a 12-kV Regaku/D-Max RA with scanning rate of 2°/min and a scanning scope from 1.0° to 40.0°. The DSC patterns were obtained on a PE DSC-7 by scanning the samples with a scanning rate from 10 to 20°C within the scope from 50 to 300°C. For comparison of the crystallization, the samples selected are treated by dehydration under the same temperature and vacuum conditions and then scanned under the protection of N_2 gas with a flow rate 40 mL/s, which is more than used with the original samples. The step-by-step scanning process is specially designed and corrected by the tin standard after each sample.

TEM Analysis

PET samples are embedded in the epoxy and cured, which did not affect the structure as in previous reports.[23,21,44] Then, the ultrathin microtome section films (50–100 nm) are cut with a microtome diamond knife. These section films are moved to prepared copper grids of TEM. To obtain a spherulitic morphology for comparison, the section films are dyed in a vapor of OsO_4, in a cabinet for protection. TEM observation is under an operation voltage of 200 kV on a JEOL 2000.

AFM Analysis

The samples for AFM measurement are quenched, that is, adequate samples are heated 10°C above their melting points with a pressure of about 5 MPa in an oil hydraulic press and melted 5 min, then withdrawn from the press rapidly and put into mixed water and ice immediately. To do this, several attempts should be made to ensure that each sample is put into the media at nearly the same time in rapid speed. From this process, the film samples could be obtained. AFM measurement was made on a Digital Instrument (Japan Co.) Nano-III. Before AFM observation, the film surface has to be checked by optical microcopy to ensure a continuous and flat surface without breakage or damage. Among many AFM techniques, the constant-height mode is adopted to observe the molecules and atoms in the samples, that is, when probe scanning in both X and Y directions, its Z direction remains at a constant height. The signal picture in the Z direction cantilever can be recorded.

Element Analysis

The elements of N and C in the samples is measured on an element analysis device, a CHN-Autometer for elements (made in China). The principle is briefly described below:

At first, standard samples containing the elements of nitrogen (N) and carbon (C) are prepared and measured on the device above, and then the sensitivity of N (S_N) and C (S_C) for standard samples can be obtained. Based on these sensitivities, the sensitivity for practical samples could be obtained by the following equations:

$$S_i = \mu g_i / h_i \tag{1}$$

$$E_i\ (\%) = 100 \times \bar{S}_i \times h_i' / W_s \tag{2}$$

where S_i is the sensitivity of element i in practical samples; μg_i, the microgram for practical element i; h_i, peak height for practical element i subtracted from only the standard peak height; E_i, the practical element i content; $\bar{S}_i$, the means of each measured sensitivity (S_i); h'_i, the recorded peak height for practical elements; and W_s, the sample weight. For comparison, the organic molecules' weight in clay were given when we prepared these organic clays, but in the final product of organic clay, the practical organic molecules' weight in the sample should be measured, which is obtained by an attached analysis balance with an accuracy of 1/100,000 g, where the organic weight is obtained by heating an organic clay to a high temperature to 1000°C.

Heat-distortion Temperature (HDT) Analysis

The samples for HDT measurement are extruded at a temperature of 270°C in the extruding machine, and the sample size was 120 × 10 × 12 mm. The experiment was done according to the China National Standard-GB-1634-79, where the device used is defined (made in China) as the measurement media of polydialkylsiloxane. The measurement mechanism is a weight-set method, that is, the sample is set between two pivots submerged in the media of the cylinder while the weight set is exerted on the center of the samples. The weight to be exerted was 4.6 kg according to the standard. In succession, the liquid media

Table II Results of Analysis and Calculation for Reagents in Pretreated Clay

Reagents	C/N (Calculated Element Ratio)	C/N (Experimental Element Ratio)
CN-16	18.8	19.6
M-6A	6.96	6.97
EA	2.30	2.19
LLA	11.2	11.3

CN-16, $CH_3(CH_3)CN(CH_2)_{12}—CH_3$; M-6A, ε-caprolactum; EA, ethanolamine; LLA, laurilamine.

were heated in the cylinder; thus, the plastic samples will be bent and each torque is recorded by a sensitive meter attached to the pinpoint of the sample. In each measurement, two samples are used to compare the torque value in the sensitive meter. The final results are from the means of these two results.

RESULTS AND DISCUSSION

The samples of pretreated clay were dried to analyze their elements. This analysis will show how many reagents react with the cation ions located in the gallery of the lamellae by an ion-exchange process, the results of which are shown in Table II.

It is seen from Table II that the properly chosen reagents could react with or intercalate into the clay by ion exchange to a complete extent when controlling the pretreatment process of the clay. But X-ray results tell us that the intercalation could not reach a perfect degree in some adopted reagents. Figure 1(A,B) shows these comparison results, in which short-chain reagents have appeared as diffraction peaks near 7°, showing an imperfect intercalation. The results of the measurement of the polymerization samples of the polyester with pretreated clay (by LLA) are shown in Table III.

Table IV Properties of HDT and Film Product for NPET by Different Reagents

Reagents	HDT (°C)	Film Transparency
EA (1%)	84	Y
EA (3%)	89	Y
EA (5%)	95	Y/N
OT (3%)	92	Y
LLA (3–5%)	105	Y
CPL (3–5%)	l74–102	Y/N
PET	76	Y

Percent number in reagent parentheses is the clay-loading weight; EA, ethanolamine; OT, cetyltrimethylammonium salt; LLA, laurilamine; CPL, 1,6-hexanediamine.

From Table III, it is seen that the molecular weights of the nanocomposites specially chosen are nearly the same within an error scope; meanwhile, their molecular weight distribution is narrower and narrower with increase of the clay content. The intention of choosing this type of samples is expected to clarify the effect of the clay content on the physical properties of the nanocomposites and especially clarify the nanostructure effect.

Similarly, by controlling the kind of reagents used, the surface polarity of the clay will change with the reagent end groups and, thus, has a direct effect on the interaction between the treated clay and the polymer matrix. This effect is clearly seen in Table IV for the properties of the HDT. The length of the carbon chain and the polarity of a reagent have an obvious effect on the HDT; for example, for samples from EA versus

Table III Physical Properties of Nanocomposite Sample to be Investigated from Different Characterization Techniques

Sample No.	MMt Content (%)	T_m (°C)	M_w (g/mol)	M_n (g/mol)	M_w/M_n	η (dLg)
1	0.0	259.0	3.71	1.8	2.0	0.57
2	0.50	258.0	4.72	2.4	2.0	0.69
3	1.0	256.0	4.0	2.1	2.0	0.65
4	2.2	255.0	4.1	2.3	1.8	0.62
5	3.0	254.0	4.5	2.3	1.9	0.68
6	5.0	252.0	4.2	2.5	1.7	0.63

T_m, melting-point temperature, data error ±0.5°C; M_w, M_n, molecular weight by GPC; η, viscosity in solution.

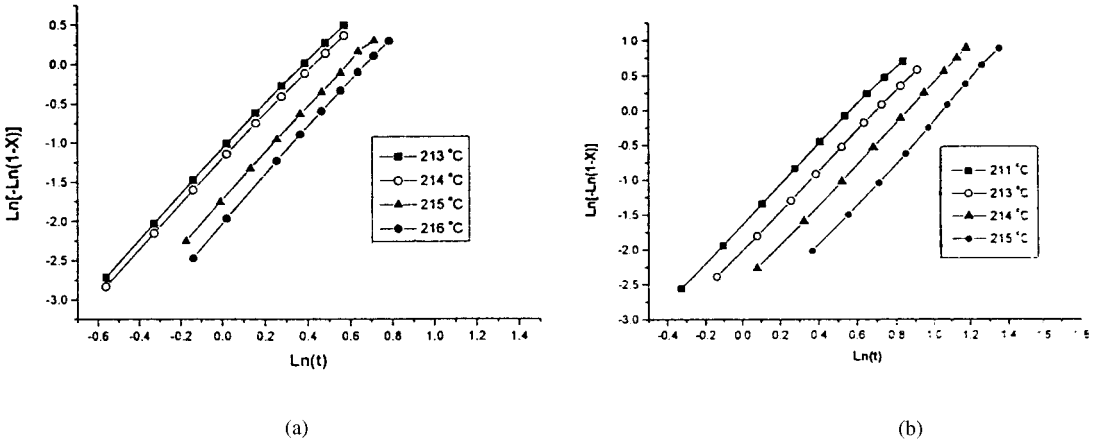

Figure 2 Plot for isothermal crystallization dynamics described by Averami equation with DSC scanning of samples 1 (a for PET) and 3 (b for PET with MMT content of 1.0%).

CPL, their final products have different HDTs due to their carbon chain length, while for samples from CPL versus LLA, their difference in the HDT resulted mainly from their polarity.

Some samples were selected to be subjected to DSC scanning, with their results shown in Figure 2, which illustrates the isothermal crystallization scanning result patterns. The results were analyzed by the Averami equation[24,27]

$$\mathrm{Ln}(-\mathrm{Ln}\{1-[x(t)]\}) = \mathrm{Ln}\ k + n\ \mathrm{Ln}\ t \qquad (3)$$

The results show that samples 1 and 2 with a low content of MMt have similar patterns. With a low MMt content, a perfect distribution could be reached.[23] Thus, from sample 2 in Figure 2, either a complete exfoliation or a weak nanostructure of MMt occurred because the low clay content did not have an obvious effect on the matrix, and, thus, the homogeneous stable system of the matrix remained unchanged (which is compared to the X-ray diffraction results in Fig. 10). But when the MMt content was more than 2.2%, approaching 3.0%, by weight, the crystallization patterns obviously changed (see Fig. 3). We can see in Figure 3, at the upper ends of the curves showing the late stage of crystallization, that bends appear compared to the straight lines seen in Figure

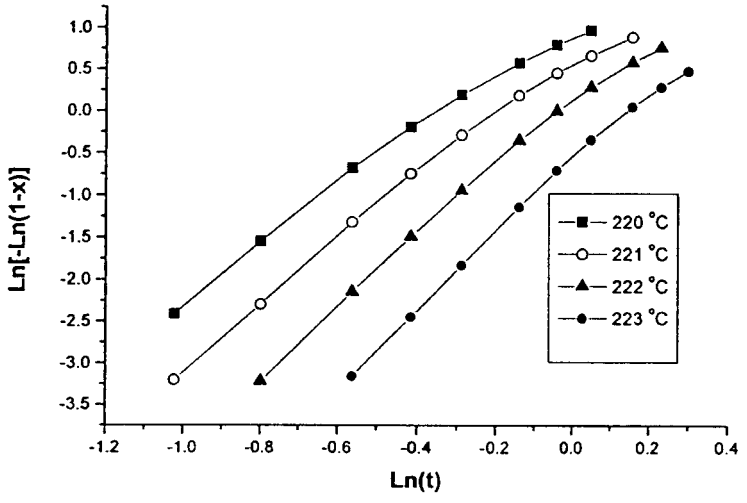

Figure 3 Plot for isothermal crystallization dynamics described by Averami equation for DSC scanning of sample 5 (PET with MMT content of 3.0%).

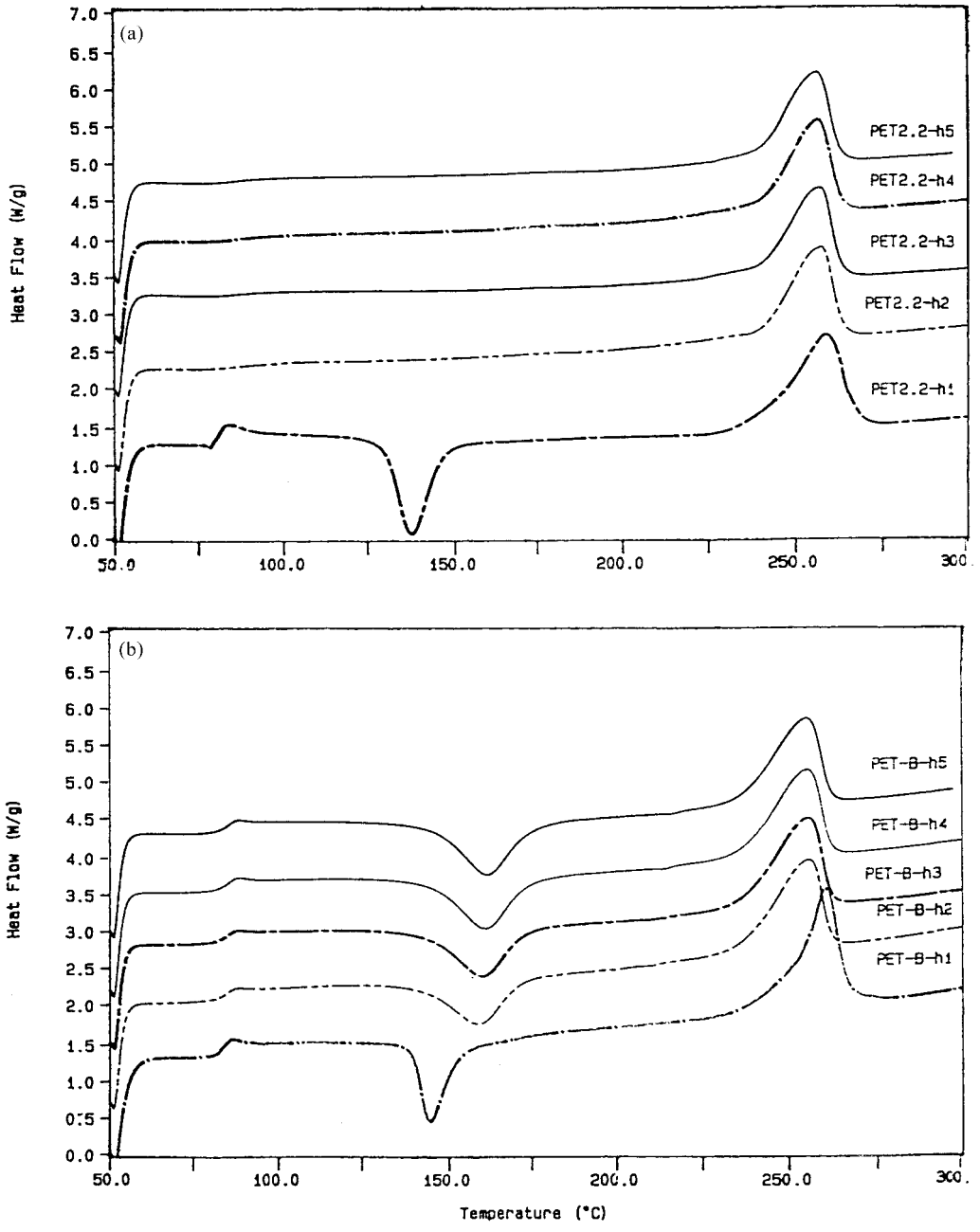

Figure 4 DSC crystallization patterns of (a) pure PET (sample 1) and (b) nanocomposite of sample 4 with MMt content of 2.2% by weight.

2; this secondary crystallization behavior shown in Figure 3 is believed to be proof that there exists a heterogeneous metastable or an unstable lamellae state in nanocomposites with a clay content exceeding some value (say 3% by weight in this article).

In fact, in previous preparation of nanocomposites, it was thought that the optimized MMt content in the composites was about 3.0% by weight. When the MMt content is more than 5.0% by weight, the agglomerated particles easily form and the heterogeneous exfoliation of lamellae may occur (see discussion below).

Figure 4 shows a comparison of a series of DSC scanning results of samples 1 (pure PET, PET-B) and 3 (PET-2.2) with a clay content of 2.2% by weight. The original scanning of h1 for sample 3 is seen to have double melting peaks and cool

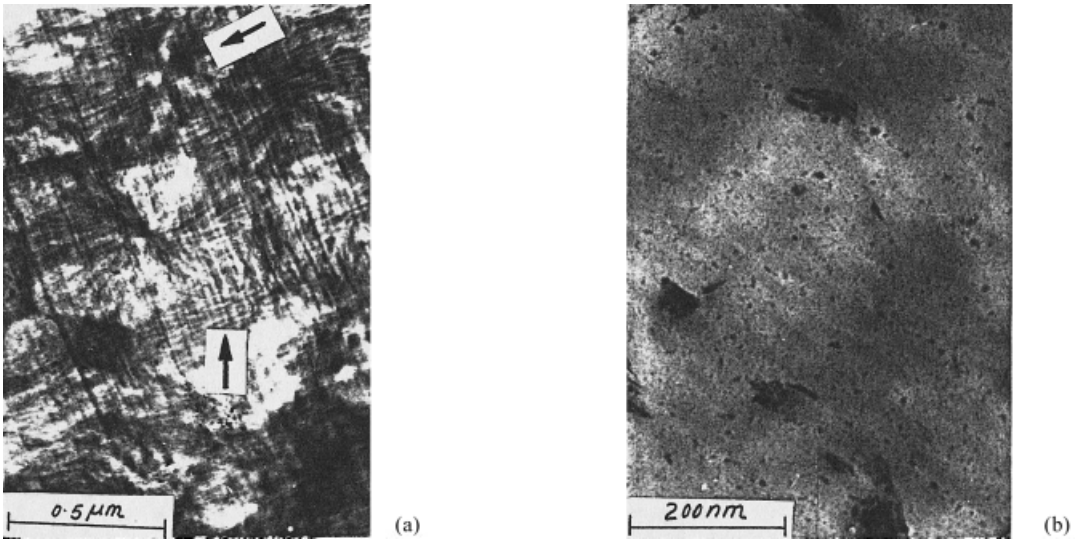

Figure 5 TEM morphology of (a) spherulite of PET and (b) disappearance of spherulite (due to hindering spherulite from growing).

crystallization peaks (near to the position of 150.0°C), similar to those of the pure PET.

The scanning results of samples 1 and 2 are clearly different in that, in the second scanning (h2), sample 1 has similar patterns in all the cool crystallization peaks, while sample 3 is without cool crystallization peaks. These scanning results show that the sample 3 nanocomposite does not go through the cool crystallization process and is straightforwardly completely crystallized, that is, the crystallization process of sample 3 is shortened compared with that of PET without clay, which is also seen in ref. 27. From this comparison, it is evident that the crystallization rate of the sample 3 nanocomposite is more rapid than that of the PET of sample 1, which is thought to be from the nucleus effect of the nanoparticles of clay or from nanoparticles combining with the polymer matrix which formed a nucleus nanostructure in the nanocomposites system.

The nanoparticles can hinder the PET crystal from growing large, that is, these nanoparticles can make the crystal much finer than that of PET. This has been reported in previous investigations of PA/MMt and/or PET/MMt nanocomposites without a controlling process and similar to works using TEM and AFM technologies.[9,23,24,26,27,34] Here, based on PET and NPET, a comparison of their morphology is shown in Figure 5, which clearly demonstrates that a spherulite morphology can be clearly seen in PET [shown by arrows in Fig. 5(a)]; the spherulites are micron-size (about 0.5 μm), but these spherulites disappear in NPET due to the nanoscale particles hindering them from growing [see Fig.5(b)]. In Figure 5(b), the particles are distributed in nanoscale, while the PET crystallites seem very fine compared with the clay particles.

There also appears an interesting phenomenon in the nanocomposites of NPET as seen in Figure 6. In Figure 6(a), some lamellae are exfoliated into mirrorlike particles with an MMt content of 2.2% by weight, but we would see a few agglomerated particles in different parts of the same samples of the nanocomposites with MMt of 3% by weight. For further understanding, different reagents of clay were tried, showing that the polarity of the reagents also affected the morphology, as shown in Figure 5, that is, the high polarity of the reagents and their being compatible with the PET chain tend to develop such a morphology as in Figure 5(a).

Figure 6 shows the nanocomposite samples with an MMt content of 3% by weight. Some of the agglomerated particles could also be found and account for approximately fewer than 1% by weight according to number statistics based on previous reports.[26] But it must be pointed out that the agglomerated particles are about 300 nm (see discussion of Fig. 7 below), which may be thought of as multistacked lamellae. These stacked lamellae may form a heterogeneous unstable zone different from that of the homogeneous zone. Figure 6 shows clearer gallery lamellae and mirror morphology than those in Figure 5. Thus, it is our thought that the agglomerated

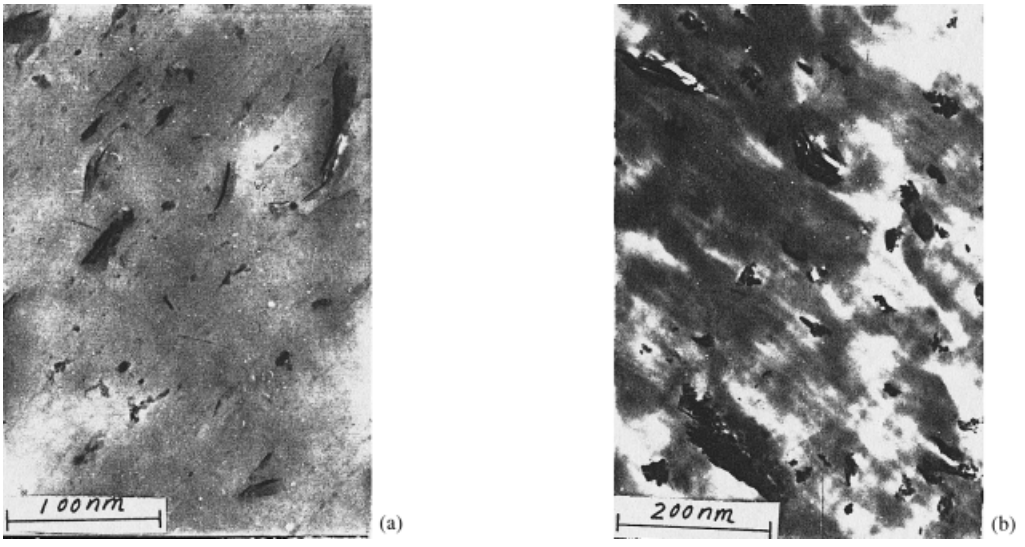

Figure 6 TEM morphology of (a) exfoliated lamellae and (b) agglomeration.

stacked lamellae may exist in the nanocomposites in one way or another depending on the preparation condition.

The formation of the mirror morphology and nanostructure scale effect may indicate why better optical properties of the nanocomposites than those of the polymer matrix could be obtained. A visible light in 400–800-nm scale can go through the nanocomposite matrix. Thus, even though some lights encounter the mirror, they can go through in a refraction manner. Due to the fine crystal size which decreases the effect of the refraction of the crystals, the nanocomposites, in some cases, could have better optical properties than those of the polymer itself (see Table I). The nanoparticle distribution of the nanocomposite sample obtained by number statistics by TEM is seen in Figure 7(a,b).

For TEM statistics, the average diameters (D) of the particles are obtained by directly measuring the cross length of the particles. Using an experimental statistical method, 600–1000 parti-

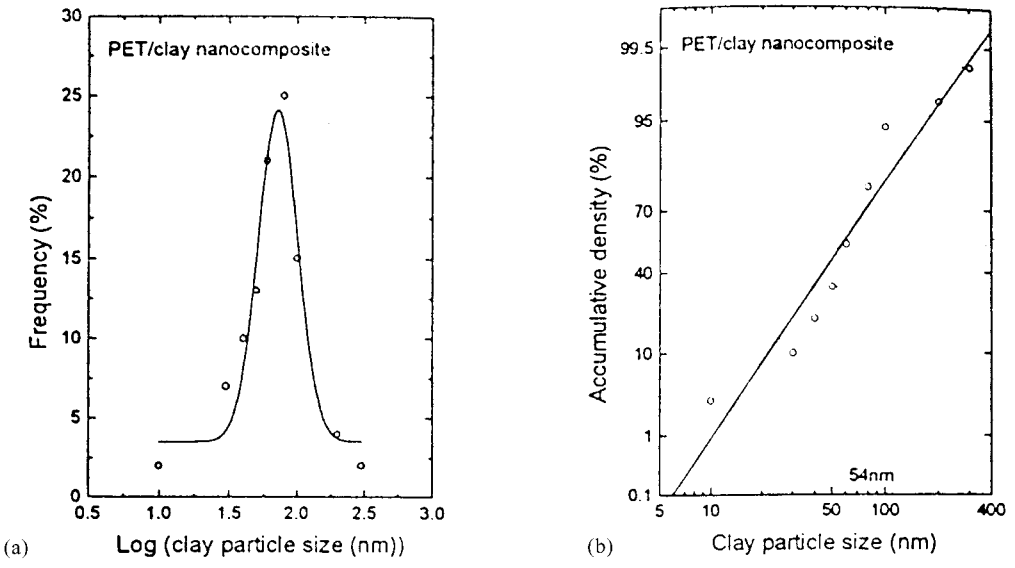

Figure 7 Plot of particle-size logarithmic normal distribution of nanocomposite sample with clay content of 2.5% (a) distribution frequency; (b) distribution accumlative density.

cles were observed, and then their arithmetic means (d_n) were multiplied by a coefficient of 1.56 to give a value of D:

$$D = 1.56 \times d_n \quad (4)$$

From Figure 7, it can be obtained from eq. (4) that the particles are in as close to a normal distribution with a greater probability distribution from 30–70 nm and a special average accumulative density of 54 nm. Thus, the nanometer particle distribution has an effect on the crystallization as described above, while Figure 8 shows the results of further investigations on the effect of MMt on the morphology of molecular chains and lamellae.

When these samples go through a quenching process, they are subjected to AFM measurement, providing a phase morphology difference between PET and NPET, that is, regular patterns for NPET were obtained, while random or amorphous patterns for PET were obtained. In observing the morphology in Figure 8(a–c), a technique of a constant-height mode is adopted to record the plot of height versus the side direction, from which the dark lamellae phase is 1.1–1.3 nm higher than is the continuum phase. For PET [Fig. 8(c)], the dark phase is thought to be composed of microcrystallites of PET chains, while in Figure 8(a,b), the dark phase or lines result from the mixing up of exfoliated MMt lamellae and microcrystallites of PET chains. Furthermore, from the force–distance curve on the right (Fig. 8), it is seen that NPET (sample 6) has a quite different curve patterns from those of PET and NPET (sample 3), showing some irregular patterns formed when clay loading was very high (e.g., 5% by weight). For a low-loading clay, the force–distance patterns are similar to those of pure PET. This should conform to the results in Figure 2. Furthermore, the average amorphous phase (chains) interdistance is 1.88 nm for NPET (sample 3) and 1.11 nm for NPET (sample 6), that is, the bright phase part became high with clay loading. This unusual phenomenon for NPET (sample 6) is caused by too much MMt lamellae loading and by the formation of agglomerations (see TEM results above). Thus, it is obvious that a too high loading of clay would cause a high density of agglomerations and nucleus centers, which would reduce the amorphous part in the nanocomposites. For example, in the amorphous phase of PET, the average interdistance between the molecular chain is 0.43 nm less than that of NPET. In NPET, a homogeneous phase composed of polymer chains and their interaction with MMt lamellae formed a nanostructure. This nanostructure phase should play the role of the nucleus for crystallization, which explains why NPET is more rapid to crystallize than is PET. The random molecular chains in PET could not organize quickly in the quenching state to form regular chains. In other words, it would take more space for molecular chain movements to form a crystal domain. While NPET chains are more regular than are those of PET, in which many molecular chain textures in a nearly parallel state could be seen (especially shown in NPET with an MMt content of 5.0% by weight). Also, the confined molecular chains by MMt lamellae in NPET are also factors for easy crystallization because there is less space for the molecular chains to move.[27,34] A mechanism to describe the morphology of NPET and PET is shown in Figure 9.

In Figure 9(A), the crystallized domain in as-polymerized PET has parallel molecular chains, but they are rapidly changed into random coil when quenched. Thus, it has too many coils to crystallize. In Figure 9(B,C), NPET molecular chain movements are obviously hindered by at least three kinds of MMt lamellae (random, parallel, and broken mirrorlike lamellae shown in Fig. 6); those chains close to the MMt lamellae surface will become harder than will the chains far away from it.[34,45] In Figure 9(B,C), the model molecular chains are lying on the surface of the MMt lamellae. It is these hard chains interacting with MMt lamellae that would crystallize more easily than would the other chains. Thus, for PET, its molecular chains can only be interacted with other molecular chains. While for NPET, even though nanoparticles in the random state are in some domain, their molecular chains are less coiled than are those of PET because the MMt lamellae there have taken up space and formed a dense system. Those molecular chains close to the surface of random lamellae would also take a regular shape and even have a greater probability to have a shape similar to those of the model plate (template) or lamellae than those of pure PET. This less coiled molecular morphology of NPET would explain why an easier crystallization of NPET than PET could occur.

Besides, it could be speculated that unstable lamellae in NPET are unavoidable due to lamellae agglomerations [see models in Fig. 9(A,B)]. From both the TEM and AFM results above, these unstable lamellae morphologies can be seen. But

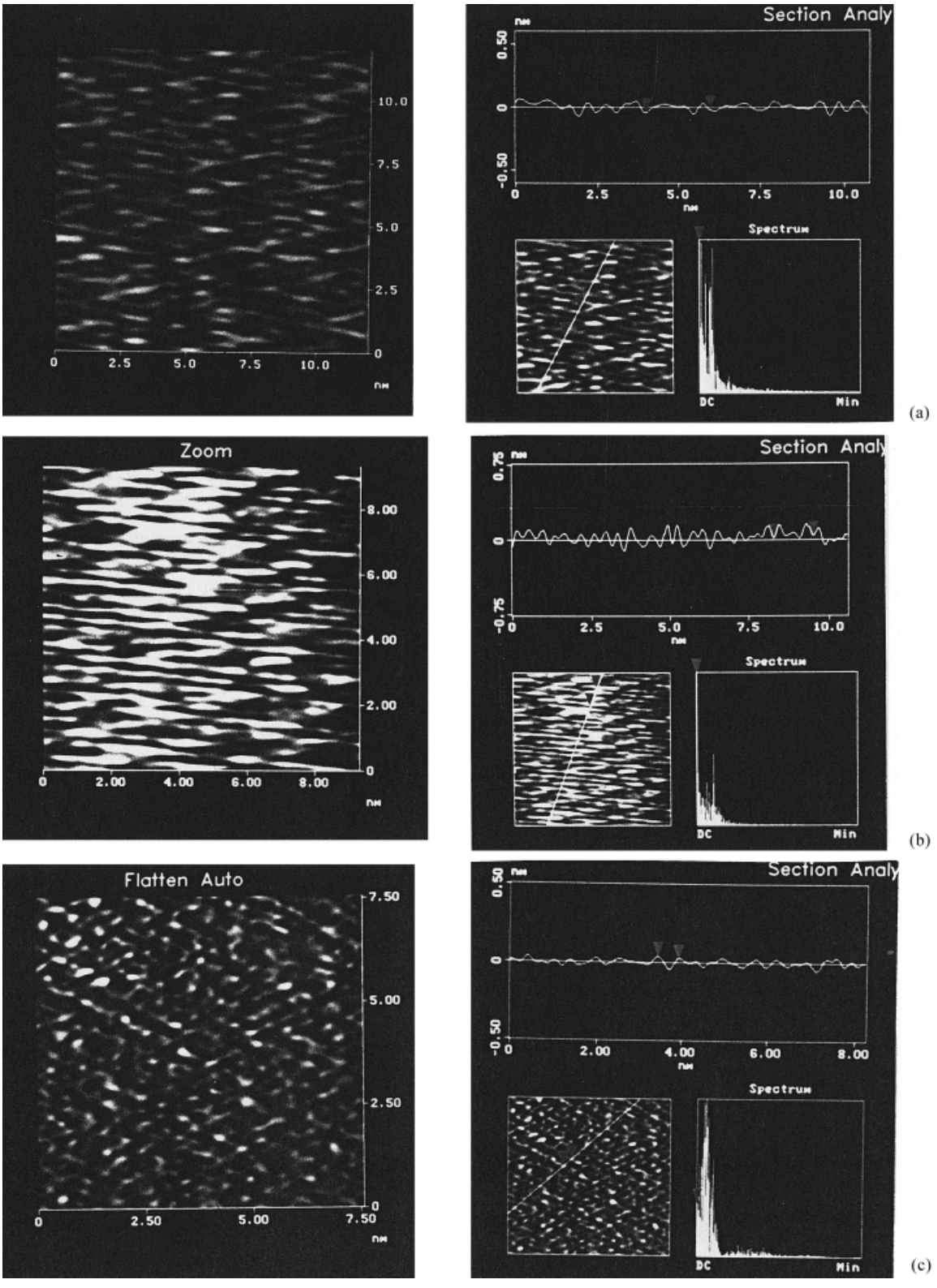

Figure 8 AFM morphology of nanocomposite polyester (a) with 1.0% content of MMt by weight and (b) with 5.0% cont. of MMt by weight and (c) pure PET.

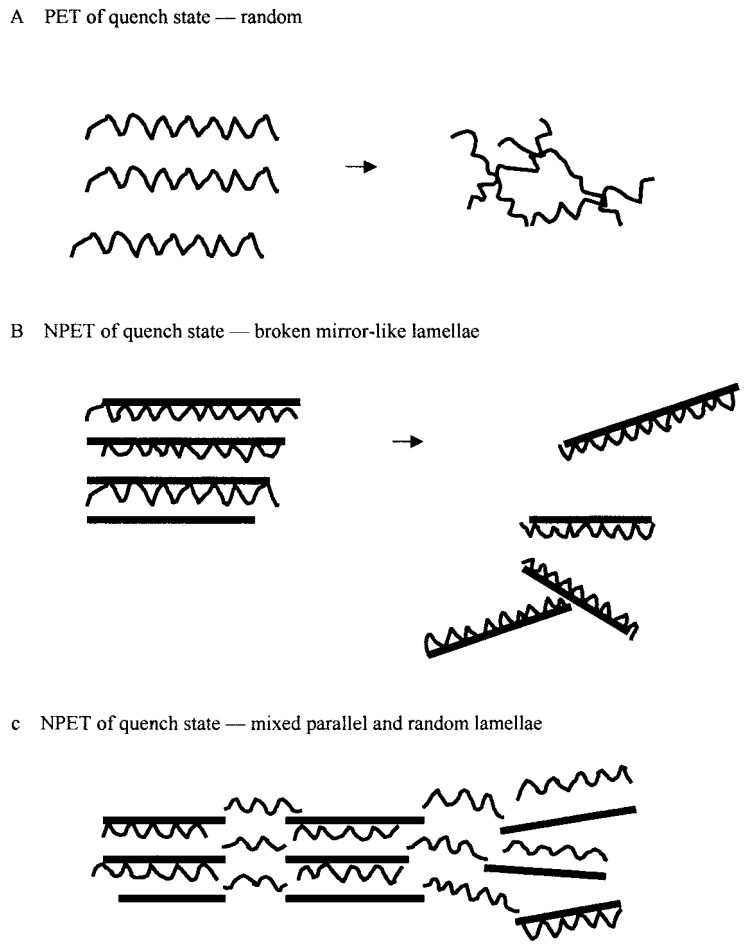

Figure 9 Morphology model of NPET and PET in quenched state.

both direct and system evidence could not be obtained so far. Thus, we only give a clue of this unstable morphology by WAXD, shown in Figure 10.

Unlike the results of previous reports,[23,24] WAXD here would give different characterization results. X-ray patterns of the as-polymerized NPET and PET samples have shown that the residue diffraction peaks from 1° to 7° [see Fig. 10(a)] nearly disappear, while, here, with the as-polymerized sample 5 (clay content of 3% by weight) several peaks from 1° to 7° appeared when it was subjected to annealing of only about 5 min at 130°C.

As shown in Figure 1, the original clay had a diffraction peak near the position of 7°. Also, for the nanocomposite NPET, diffraction peaks from 1° to 7° are related to the interlamellae distance of the gallery in MMt according to its crystal structure,[23,24] that is, the peak responds to the (001) face reflection of MMt(clay).[24,26,27,34] In Figure 10(a), it is obvious is that the peak diffraction intensity changes with the annealing time (see positions from 1° to 7°). In Figure 10, peaks X and Y are either from the diffraction of residue agglomeration of the clay (001) crystal face reflection or from another source (e.g., from a metastable state), but it seems not to be expected that peak X at 1.0° to 5.0 is from the liquid crystal (LC) state of PET due to the nature of PET itself. In our opinion, these peaks are from the mixed sources as stated above, that is, the existence of heterogeneous exfoliation of MMt lamellae (see TEM patterns above) or the existence of a heterogeneous unstable nanostructure could be thought of as the source of the phenomenon in Figure 10(a), especially when the clay content approaches some extent (over 3% by weight). Even so, this result only gives a report of this as a probable new phenomenon. As for the effect of the clay on the crystal structure of PET, it can be seen in Figure 10(b) that some splitting peaks appear

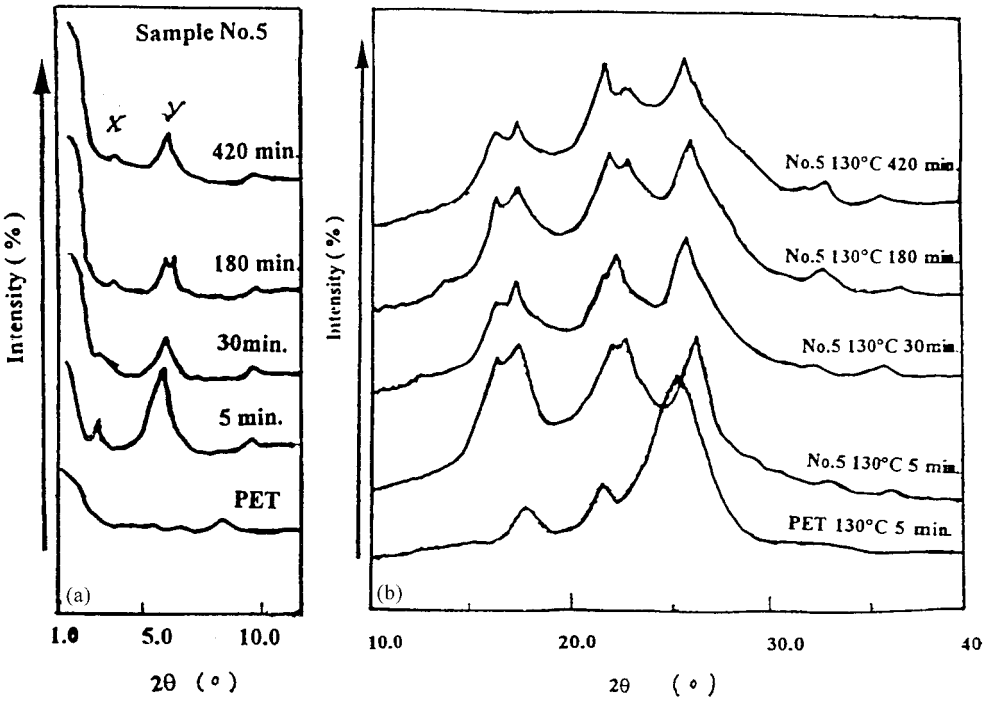

Figure 10 X-ray diffraction patterns of nanocomposite samples: (a) scanned for the lamellae structure in nanocomposites; (b) scanned for the crystal structure of PET in nanocomposites by WAXD method.

in the of 10°–25° position for the sample 5 nanocomposite. The main diffraction peak patterns remain unchanged. The splitting peaks are unstable and are merged gradually with the annealing time at 130°C, which basically shows that the crystal structure of PET is slightly affected by the addition of MMt.

CONCLUSIONS

By controlling the process of pretreatment of MMt and the nanocomposite polymerization, a more perfect morphology of the nanoparticle distribution than previously could be obtained. The nanoscale particles interact with the polymer chains to form a nanostructure, which has a great effect on the spherulite morphology, crystallization rate, HDT, and thermal properties. While the nanocomposites obtained have some unstable domains with the nanoparticles homogeneously distributed when the clay content is controlled at lower than 3% by weight, but are heterogeneously distributed when the clay content is over 3% by weight. By controlling the clay content and the methods of pretreatment and polymerization, the agglomeration of particles would not occur, while, in practice, the agglomeration particles (2% by weight of all particles) of about 300 nm or so in the nanocomposites and a nanoparticle distribution from 30 to 70 nm are often observed. Even so, it has been seen that better films and fibers made from these nanocomposite materials than those previously were provided.

Part of this work was supported by the BASF Co. by a contract between the Sino-Germany Cooperation Project and the Polyolefin National Engineering Research Center in BRICI. The support given by the National Key Basic Development Project from the Ministry of Science and Technology (Project Contract Sequence No. 1999064800) is especially appreciated by the authors.

REFERENCES

1. Ozin, G. Adv Mater 1992, 4, 612.
2. Mehnert, C. P.; Ying, J. Y. Chem Commun 1997, 2215.
3. Sellinger, A.; Weiss, P. M.; Nguyen, A.; Lu, Y.; Assink, R. A.; Gong, W.; Brinker, C. J. Nature 1998, 394, 256.

4. Toshiniko, S.; Haroon, A. U.S. Patent 5 997 958, Dec. 7, 1999.
5. Yoneda; Tadahiro; Nakahara; et al. U.S. Patent 05 863 647, Jan. 26, 1999.
6. Yoneda; Tadahiro; Nakahara; et al. U.S. Patent 05 316 714, May 31, 1994.
7. Takemura; Kazuya; Wakui; et al. U.S. Patent 05 049 295, Sept. 17, 1991.
8. Roovers; Wilhelmus, M. M.; Verhoeven; Jeroen, J. U.S. Patent 04 965 308, Oct. 23, 1990.
9. DeGuchi; et al. U.S. Patent 5 248 720, Sept. 1993 (to Ube Industries, Ltd.).
10. Hudson, S. D. U.S. Patent 5 910 523, June 8, 1999.
11. Okada, O.; et al. U.S. Patent 4 894 411, 1 /1990.
12. Yamamura; Masaaki; Inokoshi; et al. U.S. Patent 04 937 008, June 26, 1990.
13. Kamens, E. R. U.S. Patent 04 460 714, July 17, 1984.
14. Koenig, J. J.; Hsieh; H. P. U.S. Patent 04 183 843, Jan. 15, 1980.
15. Ranck, R. O. U.S. Patent 03 975 573, Aug. 17, 1976.
16. Usuki, A.; et al. J Mater Res 1993, 8, 1179–1184.
17. Kojima, Y.; et al. J Mater Res 1993, 8, 1185–1189.
18. Suzuki, K.; et al. Clays Clay Min 1988, 36, 147–152.
19. Greeland, D. J. J Colloid Sci 1963, 18, 647–664.
20. Qi; Z.; Li; Q.; Zhou, Y. Nylon6-clay, CN139643.6, 1996; p 3.
21. Vaia, R. A.; et al. Chem Mater 1993, 5, 1694–1696.
22. Vaia, R. A.; et al. Adv Mater 1995, 7, 154–156.
23. Qi, Z. N.; Ke, Y. C.; Zhou, Y. Z. Chin. Patent Appl 971 040 559.
24. Ke, Y. C.; Qi, Z. N.; Long, C. F. J Appl Polym Sci 1999.
25. Qi, Z. N.; Ke, Y. C.; Zhou, Y. Z. Chin. Patent Appl 971 041 964.
26. Ke, Y. C.; Long, C. F. In International Symposium on Polymer Physics, Guilin City, China, Nov. 25–29, 1997; p 158.
27. Ke, Y. C. Postdoctoral Research Report, Institute of Chemistry, Chinese Academy of Sciences, 1998; p 11.
28. Akelah, A.; et al. Clay Min 1994, 29, 169–178.
29. Dekking, H. G. G. Clays Clay Min 1964, 12, 603–616.
30. Kojima, Y.; et al. J Polym Sci Part B Polym Phys 1994, 32, 625–630.
31. Brindley, G. W.; et al. Clays Clay Min 1971, 18, 399–404.
32. Okada, A.; et al. J Appl Polym Sci 1989, 37, 1363–1371.
33. Usuki, A.; et al. J Mater Res 1993, 8, 1174–1178.
34. Kojima, Y.; et al. J Polym Sci Part A Polym Chem 1993, 31, 1755–1758.
35. Theng, B. K. G. Clays Clay Min 1982, 30, 1–9.
36. Giannelis, E. P.; et al. U.S. Patent 5 032 547, July 1991.
37. Friedman, H. A.; et al. U.S. Patent 5 326 500, July 1994.
38. Friedman, H. A.; et al. U.S. Patent 5 340 558, Aug. 1994.
39. Maxfield, et al. U.S. Patent 5 385 776, Jan. 1995.
40. Miyasaka, et al. U.S. Patent 5 391 437, Feb. 2, 1995.
41. Beall, G. W.; McHenry; Tsipursky; Semeon; Lincolnwood; Sorokin; Anatoliy; Buffalo Grove; Goldman; Anatoliy; Palatine; U.S. Patent 5 578 672, June 7, 1995.
42. Usuki, et al. U.S. Patent 4 889 885, Dec. 1989 (to Kabushiki Kaisha Toyota Chuo Kenkyusho).
43. Hutton, Jr.; et al. U.S. Patent 4 920 171, Apr. 1990 (to Monadnock Paper Mills, Inc.).
44. Lincoln, D. M.; Vaia, R. A.; Wang, Z.-G.; Hsiao, B. S. Polymer 2001, 42, 1621–1631.
45. Giannelis E. P.; et al. U.S. Patent 5 032 546, July, 1991.
46. Jiang B. Z.; et al. In International Symposium on Polymer Physics, Guilin City, China, Nov. 25–29, 1997; p 174.
47. Jimenez, G.; Ogata, N.; Kawai, H.; Ogihara, T. J Appl Polym Sci 1997, 64, 2211.